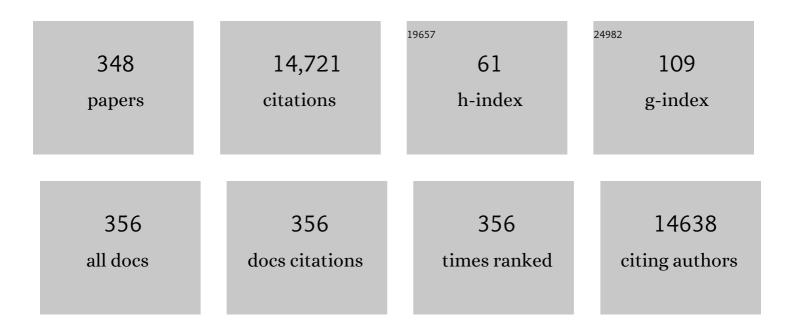
List of Publications by Year in descending order

Source: https://exaly.com/author-pdf/5096787/publications.pdf Version: 2024-02-01



#	Article	IF	CITATIONS
1	Deep Learning–based Recurrence Prediction in Patients with Non–muscle-invasive Bladder Cancer. European Urology Focus, 2022, 8, 165-172.	3.1	22
2	EDTA stabilizes the concentration of platelet-derived extracellular vesicles during blood collection and handling. Platelets, 2022, 33, 764-771.	2.3	12
3	Quantitative Fluorescence Imaging of Perfusion—An Algorithm to Predict Anastomotic Leakage. Life, 2022, 12, 249.	2.4	3
4	Computed Tomography–Mediated Registration of Trapeziometacarpal Articular Cartilage Using Intraarticular Optical Coherence Tomography and Cryomicrotome Imaging: A Cadaver Study. Cartilage, 2021, 13, 563S-570S.	2.7	1
5	Quantification of Light Scattering Detection Efficiency and Background in Flow Cytometry. Cytometry Part A: the Journal of the International Society for Analytical Cytology, 2021, 99, 671-679.	1.5	6
6	Quantitative change of perfusion in gastric tube reconstruction by sidestream dark field microscopy (SDF) after esophagectomy, a prospective in-vivo cohort study. European Journal of Surgical Oncology, 2021, 47, 1034-1041.	1.0	8
7	Bayesian analysis of depth resolved OCT attenuation coefficients. Scientific Reports, 2021, 11, 2263.	3.3	6
8	Toward improved endoscopic surveillance with multidiameter single fiber reflectance spectroscopy in patients with Barrett's esophagus. Journal of Biophotonics, 2021, 14, e202000351.	2.3	4
9	Experimental validation of a recently developed model for single-fiber reflectance spectroscopy. Journal of Biomedical Optics, 2021, 26, .	2.6	6
10	The compatibility of immunolabeling with STR profiling. Forensic Science International: Genetics, 2021, 52, 102485.	3.1	3
11	Misinterpretation of solid sphere equivalent refractive index measurements and smallest detectable diameters of extracellular vesicles by flow cytometry. Scientific Reports, 2021, 11, 24151.	3.3	9
12	Validation of Confocal Laser Endomicroscopy Features of Bladder Cancer: The Next Step Towards Real-time Histologic Grading. European Urology Focus, 2020, 6, 81-87.	3.1	26
13	Synchronized Rayleigh and Raman scattering for the characterization of single optically trapped extracellular vesicles. Nanomedicine: Nanotechnology, Biology, and Medicine, 2020, 24, 102109.	3.3	21
14	Comparison of Optical Imaging Techniques to Quantitatively Assess the Perfusion of the Gastric Conduit during Oesophagectomy. Applied Sciences (Switzerland), 2020, 10, 5522.	2.5	6
15	Effect of probe pressure on skin tissue optical properties measurement using multi-diameter single fiber reflectance spectroscopy. JPhys Photonics, 2020, 2, 034008.	4.6	5
16	Detection of extracellular vesicles in plasma and urine of prostate cancer patients by flow cytometry and surface plasmon resonance imaging. PLoS ONE, 2020, 15, e0233443.	2.5	17
17	Labelâ€free identification and chemical characterisation of single extracellular vesicles and lipoproteins by synchronous Rayleigh and Raman scattering. Journal of Extracellular Vesicles, 2020, 9, 1730134.	12.2	37
18	Enâ€face optical coherence tomography for the detection of cancer in prostatectomy specimens: Quantitative analysis in 20 patients. Journal of Biophotonics, 2020, 13, e201960105.	2.3	0

#	Article	IF	CITATIONS
19	A Systematic Approach to Improve Scatter Sensitivity of a Flow Cytometer for Detection of Extracellular Vesicles. Cytometry Part A: the Journal of the International Society for Analytical Cytology, 2020, 97, 582-591.	1.5	18
20	Automated Detection and Grading of Non–Muscle-Invasive Urothelial Cell Carcinoma of the Bladder. American Journal of Pathology, 2020, 190, 1483-1490.	3.8	34
21	Cancer-ID: Toward Identification of Cancer by Tumor-Derived Extracellular Vesicles in Blood. Frontiers in Oncology, 2020, 10, 608.	2.8	20
22	Subdiffuse scattering model for single fiber reflectance spectroscopy. Journal of Biomedical Optics, 2020, 25, 1.	2.6	10
23	Parametric imaging of attenuation by optical coherence tomography: review of models, methods, and clinical translation. Journal of Biomedical Optics, 2020, 25, 1.	2.6	51
24	Subdiffuse scattering and absorption model for single fiber reflectance spectroscopy. Biomedical Optics Express, 2020, 11, 6620.	2.9	8
25	Analytical model for diffuse reflectance in single fiber reflectance spectroscopy. Optics Letters, 2020, 45, 2078.	3.3	10
26	Recurrence in Non-Muscle Invasive Bladder Cancer Patients: External Validation of the EORTC, CUETO and EAU Risk Tables and Towards a Non-Linear Survival Model. Bladder Cancer, 2020, 6, 277-284.	0.4	0
27	3D co-registration algorithm for catheter-based optical coherence tomography. OSA Continuum, 2020, 3, 2707.	1.8	2
28	Limitations of Dutch Growth Research Foundation Commercial Software Weight Velocity for Age Standard Deviation Score. American Journal of Case Reports, 2020, 21, e925551.	0.8	0
29	Limitations of Dutch Growth Research Foundation Commercial Software Weight Velocity for Age Standard Deviation Score. American Journal of Case Reports, 2020, 21, e925551.	0.8	0
30	Pilot feasibility study of in vivo intraoperative quantitative optical coherence tomography of human brain tissue during glioma resection. Journal of Biophotonics, 2019, 12, e201900037.	2.3	38
31	Refractive index to evaluate staining specificity of extracellular vesicles by flow cytometry. Journal of Extracellular Vesicles, 2019, 8, 1643671.	12.2	48
32	Estimation of microvascular perfusion after esophagectomy: a quantitative model of dynamic fluorescence imaging. Medical and Biological Engineering and Computing, 2019, 57, 1889-1900.	2.8	11
33	Toward Automated <i>In Vivo</i> Bladder Tumor Stratification Using Confocal Laser Endomicroscopy. Journal of Endourology, 2019, 33, 930-937.	2.1	13
34	Deep learning for automatic Gleason pattern classification for grade group determination of prostate biopsies. Virchows Archiv Fur Pathologische Anatomie Und Physiologie Und Fur Klinische Medizin, 2019, 475, 77-83.	2.8	94
35	Weight velocity equations with 14–448â€ ⁻ days time separated weights should not be used for infants under 3†years of age. Medical Hypotheses, 2019, 129, 109234.	1.5	3
36	The First <i>In Vivo</i> Needleâ€Based Optical Coherence Tomography in Human Prostate: A Safety and Feasibility Study. Lasers in Surgery and Medicine, 2019, 51, 390-398.	2.1	9

#	Article	IF	CITATIONS
37	Optical coherence tomography to detect acute esophageal radiationâ€induced damage in mice: A validation study. Journal of Biophotonics, 2019, 12, e201800440.	2.3	5
38	Refractive index measurement using single fiber reflectance spectroscopy. Journal of Biophotonics, 2019, 12, e201900019.	2.3	21
39	Three-dimensional histopathological reconstruction of bladder tumours. Diagnostic Pathology, 2019, 14, 25.	2.0	18
40	Grading upper tract urothelial carcinoma with the attenuation coefficient of inâ€vivo optical coherence tomography. Lasers in Surgery and Medicine, 2019, 51, 399-406.	2.1	13
41	Estimating the Time of Deposition of Semen Traces using Fluorescence Protein–Lipid Oxidation Signatures. Analytical Chemistry, 2019, 91, 3204-3208.	6.5	9
42	Limitations of Weight Velocity Analysis by Commercial Computer Program Growth Analyser Viewer Edition. Annals of Biomedical Engineering, 2019, 47, 297-305.	2.5	3
43	Multiplex body fluid identification using surface plasmon resonance imaging with principal component analysis. Sensors and Actuators B: Chemical, 2019, 283, 355-362.	7.8	13
44	Oneâ€ŧoâ€one registration of enâ€face optical coherence tomography attenuation coefficients with histology of a prostatectomy specimen. Journal of Biophotonics, 2019, 12, e201800274.	2.3	10
45	Prediction of DNA concentration in fingermarks using autofluorescence properties. Forensic Science International, 2019, 295, 128-136.	2.2	10
46	Decreasing the Size of a Spectral Domain Optical Coherence Tomography System With Cascaded Arrayed Waveguide Gratings in a Photonic Integrated Circuit. IEEE Journal of Selected Topics in Quantum Electronics, 2019, 25, 1-9.	2.9	11
47	Multidiameter single-fiber reflectance spectroscopy of heavily pigmented skin: modeling the inhomogeneous distribution of melanin. Journal of Biomedical Optics, 2019, 24, 1.	2.6	9
48	Simple and robust calibration procedure for k-linearization and dispersion compensation in optical coherence tomography. Journal of Biomedical Optics, 2019, 24, 1.	2.6	23
49	Improved forward scatter detection of a flow cytometer for detection of extracellular vesicles. , 2019, , .		0
50	Pathlength distribution of (sub)diffusively reflected light. , 2019, , .		1
51	Intraoperative evaluation of perfusion in free flap surgery: A systematic review and metaâ€analysis. Microsurgery, 2018, 38, 804-818.	1.3	44
52	Standardization of extracellular vesicle measurements by flow cytometry through vesicle diameter approximation. Journal of Thrombosis and Haemostasis, 2018, 16, 1236-1245.	3.8	130
53	Comparison of Generic Fluorescent Markers for Detection of Extracellular Vesicles by Flow Cytometry. Clinical Chemistry, 2018, 64, 680-689.	3.2	76
54	Sex determination from fingermarks using fluorescent <i>in situ</i> hybridization. Analytical Methods, 2018, 10, 1413-1419.	2.7	6

#	Article	IF	CITATIONS
55	On-chip Mach-Zehnder interferometer for OCT systems. Advanced Optical Technologies, 2018, 7, 103-106.	1.7	11
56	Absolute sizing and label-free identification of extracellular vesicles by flow cytometry. Nanomedicine: Nanotechnology, Biology, and Medicine, 2018, 14, 801-810.	3.3	105
57	Optical techniques for perfusion monitoring of the gastric tube after esophagectomy: a review of technologies and thresholds. Ecological Management and Restoration, 2018, 31, .	0.4	41
58	Effect of ephedrine on gastric conduit perfusion measured by laser speckle contrast imaging after esophagectomy: a prospective in vivo cohort study. Ecological Management and Restoration, 2018, 31, .	0.4	9
59	An In-vivo Prospective Study of the Diagnostic Yield and Accuracy of Optical Biopsy Compared with Conventional Renal Mass Biopsy for the Diagnosis of Renal Cell Carcinoma: The Interim Analysis. European Urology Focus, 2018, 4, 978-985.	3.1	9
60	Dual excitation wavelength system for combined fingerprint and high wavenumber Raman spectroscopy. Analyst, The, 2018, 143, 6049-6060.	3.5	30
61	VS03.01: QUANTITATIVE IMAGING OF CHANGE IN MICROCIRCULATION BY SIDESTREAM DARK FIELD MICROSCOPY (SDF) AFTER ESOPHAGECTOMY. Ecological Management and Restoration, 2018, 31, 47-48.	0.4	0
62	FA05.03: EFFECT OF EPHEDRINE ON GASTRIC CONDUIT PERFUSION MEASURED BY LASER SPECKLE CONTRAST IMAGING (LSCO) AFTER ESOPHAGECTOMY: A PROSPECTIVE IN-VIVO COHORT STUDY. Ecological Management and Restoration, 2018, 31, 10-10.	0.4	2
63	PS01.186: QUANTITATIVE PERFUSION EVALUATION AFTER GASTRIC TUBE RECONSTRUCTION USING FLUORESCENCE IMACING. Ecological Management and Restoration, 2018, 31, 102-103.	0.4	1
64	Centrifugation affects the purity of liquid biopsyâ€based tumor biomarkers. Cytometry Part A: the Journal of the International Society for Analytical Cytology, 2018, 93, 1207-1212.	1.5	37
65	Deriving Extracellular Vesicle Size From Scatter Intensities Measured by Flow Cytometry. Current Protocols in Cytometry, 2018, 86, e43.	3.7	47
66	Identification and detection of protein markers to differentiate between forensically relevant body fluids. Forensic Science International, 2018, 290, 196-206.	2.2	25
67	Feasibility of Optical Coherence Tomography (OCT) for Intra-Operative Detection of Blood Flow during Gastric Tube Reconstruction. Sensors, 2018, 18, 1331.	3.8	11
68	Feasibility of using optical coherence tomography to detect radiation-induced fibrosis and residual cancer extent after neoadjuvant chemo-radiation therapy: an ex vivo study. Biomedical Optics Express, 2018, 9, 4196.	2.9	4
69	Hollow organosilica beads as reference particles for optical detection of extracellular vesicles. Journal of Thrombosis and Haemostasis, 2018, 16, 1646-1655.	3.8	44
70	Periocular CO ₂ laser resurfacing: severe ocular complications from multiple unintentional laser impacts on the protective metal eye shields. Lasers in Surgery and Medicine, 2018, 50, 980-986.	2.1	13
71	Feasibility of using optical coherence tomography to detect acute radiation-induced esophageal damage in small animal models. Journal of Biomedical Optics, 2018, 23, 1.	2.6	5
72	Needle-based optical coherence tomography for the detection of prostate cancer: a visual and quantitative analysis in 20 patients. Journal of Biomedical Optics, 2018, 23, 1.	2.6	17

#	Article	IF	CITATIONS
73	Confocal Laser Endomicroscopy for the Diagnosis of Urothelial Carcinoma in the Bladder and the Upper Urinary Tract: Protocols for Two Prospective Explorative Studies. JMIR Research Protocols, 2018, 7, e34.	1.0	13
74	Confocal Laser Endomicroscopy and Optical Coherence Tomography for the Diagnosis of Prostate Cancer: A Needle-Based, In Vivo Feasibility Study Protocol (IDEAL Phase 2A). JMIR Research Protocols, 2018, 7, e132.	1.0	7
75	Ex-vivo study in nephroureterectomy specimens defining the role of 3-D upper urinary tract visualization using optical coherence tomography and endoluminal ultrasound. Journal of Medical Imaging, 2018, 5, 1.	1.5	3
76	Spectral domain, common path OCT in a handheld PIC based system. , 2018, , .		2
77	Customized Tool for the Validation of Optical Coherence Tomography in Differentiation of Prostate Cancer. Technology in Cancer Research and Treatment, 2017, 16, 57-65.	1.9	13
78	Noninvasive fluence rate mapping in living tissues using magnetic resonance thermometry. Journal of Biomedical Optics, 2017, 22, 036001.	2.6	3
79	Methodological Guidelines to Study Extracellular Vesicles. Circulation Research, 2017, 120, 1632-1648.	4.5	728
80	Modeling subdiffusive light scattering by incorporating the tissue phase function and detector numerical aperture. Journal of Biomedical Optics, 2017, 22, 050501.	2.6	17
81	Integrated-optics based multi-beam imaging for speed improvement of OCT systems. Proceedings of SPIE, 2017, , .	0.8	Ο
82	Visibility of fiducial markers used for imageâ€guided radiation therapy on optical coherence tomography for registration with <scp>CT</scp> : An esophageal phantom study. Medical Physics, 2017, 44, 6570-6582.	3.0	10
83	Surface Plasmon Resonance is an Analytically Sensitive Method for Antigen Profiling of Extracellular Vesicles. Clinical Chemistry, 2017, 63, 1633-1641.	3.2	31
84	OCT Amplitude and Speckle Statistics of Discrete Random Media. Scientific Reports, 2017, 7, 14873.	3.3	34
85	Autofluorescence imaging for improved visualization of joint structures during arthroscopic surgery. Journal of Experimental Orthopaedics, 2017, 4, 19.	1.8	4
86	Current position of diagnostics and surgical treatment for upper tract urothelial carcinoma. Minerva Urology and Nephrology, 2017, 69, 159-165.	2.5	4
87	Can we predict necrosis intra-operatively? Real-time optical quantitative perfusion imaging in surgery: study protocol for a prospective, observational, in vivo pilot study. Pilot and Feasibility Studies, 2017, 3, 65.	1.2	9
88	Single fiber reflectance spectroscopy calibration. Journal of Biomedical Optics, 2017, 22, 1.	2.6	13
89	Special Section Guest Editorial: Commemorating 25 Years of Optical Coherence Tomography: a Perspective on Biomedical Applications. Journal of Biomedical Optics, 2017, 22, 1.	2.6	1
90	Quantitative attenuation analysis for identification of early Barrett's neoplasia in volumetric laser endomicroscopy. Journal of Biomedical Optics, 2017, 22, 086001.	2.6	10

#	Article	IF	CITATIONS
91	Applicability of quantitative optical imaging techniques for intraoperative perfusion diagnostics: a comparison of laser speckle contrast imaging, sidestream dark-field microscopy, and optical coherence tomography. Journal of Biomedical Optics, 2017, 22, 1.	2.6	12
92	Irreversible Electroporation for the Ablation of Renal Cell Carcinoma: A Prospective, Human, In Vivo Study Protocol (IDEAL Phase 2b). JMIR Research Protocols, 2017, 6, e21.	1.0	18
93	Assesment of apoptosis induced changes in scattering using optical coherence tomography. Journal of Biophotonics, 2016, 9, 913-923.	2.3	8
94	Wound scabs protect regenerating tissue against harmful ultraviolet radiation. Medical Hypotheses, 2016, 96, 39-41.	1.5	1
95	Prostate cancer diagnosis by optical coherence tomography: First results from a needle based optical platform for tissue sampling. Journal of Biophotonics, 2016, 9, 490-498.	2.3	24
96	Optical Coherence Tomography as a Tool for InÂVivo Staging and Grading of Upper Urinary Tract Urothelial Carcinoma: AÂStudy of Diagnostic Accuracy. Journal of Urology, 2016, 196, 1749-1755.	0.4	38
97	Measurement of biofilm growth and local hydrodynamics using optical coherence tomography. Biomedical Optics Express, 2016, 7, 3508.	2.9	20
98	Quantitative blood flow velocity imaging using laser speckle flowmetry. Scientific Reports, 2016, 6, 25258.	3.3	58
99	Volumetric laser endomicroscopy in Barrett's esophagus: a feasibility study on histological correlation. Ecological Management and Restoration, 2016, 29, 505-512.	0.4	22
100	Chip based common-path optical coherence tomography system with an on-chip microlens and multi-reference suppression algorithm. Optics Express, 2016, 24, 12635.	3.4	10
101	Quantification of numerical aperture-dependence of the OCT attenuation coefficient (Conference) Tj ETQq1 1 0.	784314 rş	gBT /Overlock
102	Fluorescence characteristics of human Barrett tissue specimens grafted on chick chorioallantoic membrane. Lasers in Medical Science, 2016, 31, 137-144.	2.1	4
103	Detecting signs of retinal leakage in exudative AMD using Cirrus OCT versus SL SCAN-1, a novel integrated FD-OCT into a common slit lamp. Graefe's Archive for Clinical and Experimental Ophthalmology, 2016, 254, 37-41.	1.9	0
104	Techniques that acquire donor profiling information from fingermarks — A review. Science and Justice - Journal of the Forensic Science Society, 2016, 56, 143-154.	2.1	43
105	Quantitative Assessment of Optical Properties in Healthy Cartilage and Repair Tissue by Optical Coherence Tomography and Histology. IEEE Journal of Selected Topics in Quantum Electronics, 2016, 22, 203-209.	2.9	1
106	Percutaneous Needle Based Optical Coherence Tomography for the Differentiation of Renal Masses: a Pilot Cohort. Journal of Urology, 2016, 195, 1578-1585.	0.4	15
107	On the autofluorescence of aged fingermarks. Forensic Science International, 2016, 258, 19-25.	2.2	23
108	Detection of buried Barrett's glands after radiofrequency ablation with volumetric laser endomicroscopy. Gastrointestinal Endoscopy, 2016, 83, 80-88.	1.0	52

#	Article	IF	CITATIONS
109	The Value of Optical Coherence Tomography in Determining Surgical Margins in Squamous Cell Carcinoma of the Vulva: A Single-Center Prospective Study. International Journal of Gynecological Cancer, 2015, 25, 112-118.	2.5	14
110	Irreversible electroporation: Just another form of thermal therapy?. Prostate, 2015, 75, 332-335.	2.3	34
111	Photoacoustic image patterns of breast carcinoma and comparisons with Magnetic Resonance Imaging and vascular stained histopathology. Scientific Reports, 2015, 5, 11778.	3.3	111
112	In Vivo , Percutaneous, Needle Based, Optical Coherence Tomography of Renal Masses. Journal of Visualized Experiments, 2015, , .	0.3	10
113	Functional optical coherence tomography of pigmented lesions. Journal of the European Academy of Dermatology and Venereology, 2015, 29, 738-744.	2.4	15
114	Prostate cancer diagnosis: the feasibility of needle-based optical coherence tomography. Journal of Medical Imaging, 2015, 2, 037501.	1.5	28
115	Learning curve and interobserver variance in quantification of the optical coherence tomography attenuation coefficient. Journal of Biomedical Optics, 2015, 20, 121313.	2.6	6
116	Validation of quantitative attenuation and backscattering coefficient measurements by optical coherence tomography in the concentration-dependent and multiple scattering regime. Journal of Biomedical Optics, 2015, 20, 121314.	2.6	55
117	Comparison of optical coherence tomography and histopathology in quantitative assessment of goat talus articular cartilage. Monthly Notices of the Royal Astronomical Society: Letters, 2015, 86, 257-263.	3.3	21
118	Su1723 Atlas of High-Quality Histological Correlations of Volumetric LASER Endomicroscopy Images of Barrett's Esophagus for Identification of Early Neoplasia. Gastrointestinal Endoscopy, 2015, 81, AB391-AB392.	1.0	0
119	Irreversible electroporation of the porcine kidney: Temperature development and distribution. Urologic Oncology: Seminars and Original Investigations, 2015, 33, 168.e1-168.e7.	1.6	38
120	The efficacy and safety of irreversible electroporation for the ablation of renal masses: a prospective, human, in-vivo study protocol. BMC Cancer, 2015, 15, 165.	2.6	23
121	Simultaneous and localized measurement of diffusion and flow using optical coherence tomography. Optics Express, 2015, 23, 3448.	3.4	32
122	Visualization of Latent Blood Stains Using Visible Reflectance Hyperspectral Imaging and Chemometrics. Journal of Forensic Sciences, 2015, 60, S188-92.	1.6	23
123	Optical Diagnostics for Upper Urinary Tract Urothelial Cancer: Technology, Thresholds, and Clinical Applications. Journal of Endourology, 2015, 29, 113-123.	2.1	50
124	Optical coherence tomography accurately identifies patients with penile (pre) malignant lesions: A single center prospective study. Urology Annals, 2015, 7, 459.	0.6	6
125	Treatment of coronary bifurcation lesions with the Absorb bioresorbable vascular scaffold in combination with the Tryton dedicated coronary bifurcation stent: evaluation using two- and three-dimensional optical coherence tomography. EuroIntervention, 2015, 11, 877-884.	3.2	13
126	Ultra-compact silicon photonic integrated interferometer for swept-source optical coherence tomography. Optics Letters, 2014, 39, 5228.	3.3	43

#	Article	IF	CITATIONS
127	Quantitative comparison of analysis methods for spectroscopic optical coherence tomography: reply to comment. Biomedical Optics Express, 2014, 5, 3034.	2.9	5
128	Monte Carlo simulations shed light on Bathsheba's suspect breast. Journal of Biophotonics, 2014, 7, 323-331.	2.3	2
129	Side branch healing patterns of the Tryton dedicated bifurcation stent: a 1-year optical coherence tomography follow-up study. International Journal of Cardiovascular Imaging, 2014, 30, 1445-1456.	1.5	7
130	Reproducible extracellular vesicle size and concentration determination with tunable resistive pulse sensing. Journal of Extracellular Vesicles, 2014, 3, 25922.	12.2	126
131	A literature review and novel theoretical approach on the optical properties of whole blood. Lasers in Medical Science, 2014, 29, 453-479.	2.1	310
132	Senile retinoschisis versus retinal detachment, the additional value of peripheral retinal OCT scans (SL SCANâ€I, Topcon). Acta Ophthalmologica, 2014, 92, 221-227.	1.1	23
133	Particle size distribution of exosomes and microvesicles determined by transmission electron microscopy, flow cytometry, nanoparticle tracking analysis, and resistive pulse sensing. Journal of Thrombosis and Haemostasis, 2014, 12, 1182-1192.	3.8	698
134	Immunolabeling of fingermarks left on forensic relevant surfaces, including thermal paper. Analytical Methods, 2014, 6, 1051.	2.7	14
135	Immunolabeling and the compatibility with a variety of fingermark development techniques. Science and Justice - Journal of the Forensic Science Society, 2014, 54, 356-362.	2.1	15
136	Refractive Index Determination of Nanoparticles in Suspension Using Nanoparticle Tracking Analysis. Nano Letters, 2014, 14, 6195-6201.	9.1	161
137	Oxidation Monitoring by Fluorescence Spectroscopy Reveals the Age of Fingermarks. Angewandte Chemie - International Edition, 2014, 53, 6272-6275.	13.8	51
138	Comparison of retinal nerve fiber layer thickness measurements by spectralâ€domain optical coherence tomography systems using a phantom eye model. Journal of Biophotonics, 2013, 6, 314-320.	2.3	19
139	Infrared Imaging of the Crime Scene: Possibilities and Pitfalls. Journal of Forensic Sciences, 2013, 58, 1156-1162.	1.6	27
140	Simultaneous labeling of multiple components in a single fingermark. Forensic Science International, 2013, 232, 173-179.	2.2	24
141	Dependent and multiple scattering in transmission and backscattering optical coherence tomography. Optics Express, 2013, 21, 29145.	3.4	51
142	Volumetric InÂVivo Visualization of Upper Urinary Tract Tumors Using Optical Coherence Tomography: A Pilot Study. Journal of Urology, 2013, 190, 2236-2242.	0.4	66
143	An optimized ultrasound detector for photoacoustic breast tomography. Medical Physics, 2013, 40, 032901.	3.0	41
144	Evaluation of superparamagnetic iron oxide nanoparticles (Endorem®) as a photoacoustic contrast agent for intraâ€operative nodal staging. Contrast Media and Molecular Imaging, 2013, 8, 83-91.	0.8	63

0

#	Article	IF	CITATIONS
145	Su1451 Endoscopic Multi-Wavelength Autofluorescence Spectroscopy Can Adequately Identify Premalignant Lesions in Barrett's Esophagus. Gastrointestinal Endoscopy, 2013, 77, AB328.	1.0	0
146	Successful treatment of a long tapered lesion with two overlapping ABSORB® bioresorbable vascular scaffolds of different diameters: Evaluation by three-dimensional optical coherence tomography. International Journal of Cardiology, 2013, 165, e26-e27.	1.7	5
147	The Compatibility of Fingerprint Visualization Techniques with Immunolabeling. Journal of Forensic Sciences, 2013, 58, 999-1002.	1.6	21
148	Optical biopsy of epithelial cancers by optical coherence tomography (OCT). Lasers in Medical Science, 2013, 29, 1297-305.	2.1	40
149	Design considerations for ultrasound detectors in photoacoustic breast imaging. , 2013, , .		1
150	Diffuse reflectance relations based on diffusion dipole theory for large absorption and reduced scattering. Journal of Biomedical Optics, 2013, 18, 087007.	2.6	1
151	Quantitative laser speckle flowmetry of the in vivo microcirculation using sidestream dark field microscopy. Biomedical Optics Express, 2013, 4, 2347.	2.9	30
152	Design and evaluation of a laboratory prototype system for 3D photoacoustic full breast tomography. Biomedical Optics Express, 2013, 4, 2555.	2.9	36
153	Quantitative comparison of analysis methods for spectroscopic optical coherence tomography. Biomedical Optics Express, 2013, 4, 2570.	2.9	33
154	Optimized endoscopic autofluorescence spectroscopy for the identification of premalignant lesions in Barrett's oesophagus. European Journal of Gastroenterology and Hepatology, 2013, 25, 1442-1449.	1.6	8
155	Localized measurement of longitudinal and transverse flow velocities in colloidal suspensions using optical coherence tomography. Physical Review E, 2013, 88, 042312.	2.1	55
156	The â€~nanobig rod' class of gold nanorods: optimized dimensions for improved <i>in vivo</i> therapeutic and imaging efficacy. Nanotechnology, 2013, 24, 215102.	2.6	10
157	A custom-made linear array transducer for photoacoustic breast imaging. , 2012, , .		1
158	Detection of early-stage age related macular degeneration with a compact rarebit test. British Journal of Ophthalmology, 2012, 96, 1354-1355.	3.9	4
159	Multiple scattering effects in Doppler optical coherence tomography of flowing blood. Physics in Medicine and Biology, 2012, 57, 1907-1917.	3.0	16
160	Limitations and Opportunities of Transcutaneous Bilirubin Measurements. Pediatrics, 2012, 129, 689-694.	2.1	60
161	Integrated-optics-based swept-source optical coherence tomography. Optics Letters, 2012, 37, 4820.	3.3	44

Photoacoustic detection of iron oxide nanoparticles in resected rat lymph nodes. , 2012, , .

#	Article	IF	CITATIONS
163	Spectral domain detection in low-coherence spectroscopy. Biomedical Optics Express, 2012, 3, 2263.	2.9	14
164	Visualizing breast cancer using the Twente photoacoustic mammoscope: What do we learn from twelve new patient measurements?. Optics Express, 2012, 20, 11582.	3.4	185
165	Optical coherence tomography in vulvar intraepithelial neoplasia. Journal of Biomedical Optics, 2012, 17, 116022.	2.6	35
166	In-situ imaging of articular cartilage of the first carpometacarpal joint using co-registered optical coherence tomography and computed tomography. Journal of Biomedical Optics, 2012, 17, 060501.	2.6	17
167	Adapted directivity approach for photoacoustic imaging reconstruction. Proceedings of SPIE, 2012, , .	0.8	Ο
168	Toward Spectral-Domain Optical Coherence Tomography on a Chip. IEEE Journal of Selected Topics in Quantum Electronics, 2012, 18, 1223-1233.	2.9	45
169	Hyperspectral imaging for non-contact analysis of forensic traces. Forensic Science International, 2012, 223, 28-39.	2.2	223
170	Hyperspectral imaging for the age estimation of blood stains at the crime scene. Forensic Science International, 2012, 223, 72-77.	2.2	93
171	Functional Optical Biopsy of epithelial tumors. , 2012, , .		Ο
172	Doppler-based lateral motion tracking for optical coherence tomography. Optics Letters, 2012, 37, 2220.	3.3	5
173	Identification and age estimation of blood stains on colored backgrounds by near infrared spectroscopy. Forensic Science International, 2012, 220, 239-244.	2.2	81
174	First experiences of photoacoustic imaging for detection of melanoma metastases in resected human lymph nodes. Lasers in Surgery and Medicine, 2012, 44, 541-549.	2.1	45
175	Speedâ€ofâ€sound compensated photoacoustic tomography for accurate imaging. Medical Physics, 2012, 39, 7262-7271.	3.0	108
176	Raman and Fluorescence Spectral Imaging of Live Breast Cancer Cells Incubated with PEGylated Gold Nanorods. Applied Spectroscopy, 2012, 66, 66-74.	2.2	11
177	Forensic quest for age determination of bloodstains. Forensic Science International, 2012, 216, 1-11.	2.2	120
178	Single vs. swarm detection of microparticles and exosomes by flow cytometry. Journal of Thrombosis and Haemostasis, 2012, 10, 919-930.	3.8	334
179	Differentiation between normal renal tissue and renal tumours using functional optical coherence tomography: a phase I <i>in vivo</i> human study. BJU International, 2012, 110, E415-20.	2.5	61
180	How the blood pool properties at onset affect the temporal behavior of simulated bruises. Medical and Biological Engineering and Computing, 2012, 50, 165-171.	2.8	4

#	Article	IF	CITATIONS
181	FEM model based optimization of transducer geometry for photoacoustic imaging. , 2012, , .		0
182	Advanced Diagnostics in Renal Mass Using Optical Coherence Tomography: A Preliminary Report. Journal of Endourology, 2011, 25, 311-315.	2.1	43
183	Light Interactions with Gold Nanorods and Cells: Implications for Photothermal Nanotherapeutics. Nano Letters, 2011, 11, 1887-1894.	9.1	130
184	Measurements of wavelength dependent scattering and backscattering coefficients by low-coherence spectroscopy. Journal of Biomedical Optics, 2011, 16, 030503.	2.6	32
185	Optical properties of neonatal skin measured in vivo as a function of age and skin pigmentation. Journal of Biomedical Optics, 2011, 16, 097003.	2.6	38
186	Initial results of imaging melanoma metastasis in resected human lymph nodes using photoacoustic computed tomography. Journal of Biomedical Optics, 2011, 16, 096021.	2.6	44
187	Non-contact spectroscopic determination of large blood volume fractions in turbid media. Biomedical Optics Express, 2011, 2, 396.	2.9	7
188	Optical mammography combined with fluorescence imaging: lesion detection using scatterplots. Biomedical Optics Express, 2011, 2, 1007.	2.9	10
189	Passive element enriched photoacoustic computed tomography (PER PACT) for simultaneous imaging of acoustic propagation properties and light absorption. Optics Express, 2011, 19, 2093.	3.4	84
190	Determination of the scattering anisotropy with optical coherence tomography. Optics Express, 2011, 19, 6131.	3.4	64
191	Spectral domain optical coherence tomography imaging with an integrated optics spectrometer. Optics Letters, 2011, 36, 1293.	3.3	56
192	Acousto-optic-assisted diffuse optical tomography. Optics Letters, 2011, 36, 1539.	3.3	18
193	Multiple passive element enriched photoacoustic computed tomography. Optics Letters, 2011, 36, 2809.	3.3	16
194	Heartbeat-Induced Axial Motion Artifacts in Optical Coherence Tomography Measurements of the Retina. , 2011, 52, 3908.		63
195	Biphasic Oxidation of Oxy-Hemoglobin in Bloodstains. PLoS ONE, 2011, 6, e21845.	2.5	59
196	Breast imaging using the Twente photoacoustic mammoscope (PAM): new clinical measurements. , 2011, , , .		3
197	Spatial distributions of optical and acoustic properties and correlations with temperature in cyclically frozen-thawed poly(vinyl alcohol) gel breast phantoms. , 2011, , .		1
198	Absolute measurement of absorption coefficient by combining photoacoustics and acousto-optics. Proceedings of SPIE, 2011, , .	0.8	1

#	Article	IF	CITATIONS
199	Quantitative detection of gold nanoparticles on individual, unstained cancer cells by scanning electron microscopy. Journal of Microscopy, 2011, 244, 187-193.	1.8	10
200	Scanning beyond the limits of standard OCT with a Fourier domain optical coherence tomography integrated into a slit lamp: the SL SCAN-1. Eye, 2011, 25, 97-104.	2.1	11
201	Macular pigment optical density measurements: evaluation of a device using heterochromatic flicker photometry. Eye, 2011, 25, 105-112.	2.1	36
202	Blood clearance and tissue distribution of PEGylated and non-PEGylated gold nanorods after intravenous administration in rats. Nanomedicine, 2011, 6, 339-349.	3.3	136
203	Age estimation of blood stains by hemoglobin derivative determination using reflectance spectroscopy. Forensic Science International, 2011, 206, 166-171.	2.2	98
204	A clinical instrument for combined raman spectroscopyâ€optical coherence tomography of skin cancers. Lasers in Surgery and Medicine, 2011, 43, 143-151.	2.1	62
205	Gold nanorods as molecular contrast agents in photoacoustic imaging: the promises and the caveats. Contrast Media and Molecular Imaging, 2011, 6, 389-400.	0.8	104
206	Can color inhomogeneity of bruises be used to establish their age?. Journal of Biophotonics, 2011, 4, 759-767.	2.3	16
207	Imaging Tumor Vascularization for Detection and Diagnosis of Breast Cancer. Technology in Cancer Research and Treatment, 2011, 10, 607-623.	1.9	53
208	Poly(vinyl alcohol) gels as photoacoustic breast phantoms revisited. Journal of Biomedical Optics, 2011, 16, 075002.	2.6	49
209	Integrated system for combined Raman spectroscopy–spectral domain optical coherence tomography. Journal of Biomedical Optics, 2011, 16, 011007.	2.6	51
210	In vivo low-coherence spectroscopic measurements of local hemoglobin absorption spectra in human skin. Journal of Biomedical Optics, 2011, 16, 100504.	2.6	21
211	Enlarged acceptance angle of a finite size detector in photoacoustic imaging using acoustic lenses. Proceedings of SPIE, 2011, , .	0.8	4
212	Structural and biochemical characterization of the rat retina with combined Raman spectroscopy-spectral domain optical coherence tomography (RS-SDOCT). Proceedings of SPIE, 2010, , .	0.8	0
213	Comparison of scanning beam and whole field laser Doppler perfusion imaging. , 2010, , .		0
214	Differential Pathlength Spectroscopy for the Quantitation of Optical Properties of Gold Nanoparticles. ACS Nano, 2010, 4, 4081-4089.	14.6	26
215	Apoptosis- and necrosis-induced changes in light attenuation measured by optical coherence tomography. Lasers in Medical Science, 2010, 25, 259-267.	2.1	58
216	3D finite compartment modeling of formation and healing of bruises may identify methods for age determination of bruises. Medical and Biological Engineering and Computing, 2010, 48, 911-921.	2.8	22

#	Article	IF	CITATIONS
217	Photoacoustic Imaging of the Breast Using the Twente Photoacoustic Mammoscope: Present Status and Future Perspectives. IEEE Journal of Selected Topics in Quantum Electronics, 2010, 16, 730-739.	2.9	94
218	In vivo optical path lengths and path length resolved doppler shifts of multiply scattered light. Lasers in Surgery and Medicine, 2010, 42, 852-860.	2.1	2
219	Optical and nonâ€optical methods for detection and characterization of microparticles and exosomes. Journal of Thrombosis and Haemostasis, 2010, 8, 2596-2607.	3.8	454
220	Fourier Domain Optical Coherence Tomography integrated into a slit lamp; a novel technique combining anterior and posterior segment OCT. Eye, 2010, 24, 980-984.	2.1	12
221	Quantitative measurement of attenuation coefficients of bladder biopsies using optical coherence tomography for grading urothelial carcinoma of the bladder. Journal of Biomedical Optics, 2010, 15, 066013.	2.6	64
222	A clinical probe for combined Raman spectroscopy-optical coherence tomography (RS-OCT) of the skin cancers. , 2010, , .		2
223	Path-Length-Resolved Diffusive Particle Dynamics in Spectral-Domain Optical Coherence Tomography. Physical Review Letters, 2010, 105, 198302.	7.8	42
224	Optical phantoms of varying geometry based on thin building blocks with controlled optical properties. Journal of Biomedical Optics, 2010, 15, 025001.	2.6	115
225	Feasibility of noncontact piezoelectric detection of photoacoustic signals in tissue-mimicking phantoms. Journal of Biomedical Optics, 2010, 15, 055011.	2.6	18
226	Quantitative comparison of the OCT imaging depth at 1300 nm and 1600 nm. Biomedical Optics Express, 2010, 1, 176.	2.9	81
227	lodide Impurities in Hexadecyltrimethylammonium Bromide (CTAB) Products: Lotâ^'Lot Variations and Influence on Gold Nanorod Synthesis. Langmuir, 2010, 26, 5050-5055.	3.5	73
228	Measurement of particle flux in a static matrix with suppressed influence of optical properties, using low coherence interferometry. Optics Express, 2010, 18, 2849.	3.4	7
229	Multiple and dependent scattering effects in Doppler optical coherence tomography. Optics Express, 2010, 18, 3883.	3.4	54
230	Relation between the contrast in time integrated dynamic speckle patterns an the power spectral density of their temporal intensity fluctuations. Optics Express, 2010, 18, 21883.	3.4	9
231	SiON Integrated Optics Elliptic Couplers for Fizeau-Based Optical Coherence Tomography. Journal of Lightwave Technology, 2010, 28, 2836-2842.	4.6	10
232	Burn imaging with a whole field laser Doppler perfusion imager based on a CMOS imaging array. Burns, 2010, 36, 389-396.	1.9	11
233	<i>In vitro</i> toxicity studies of polymer-coated gold nanorods. Nanotechnology, 2010, 21, 145101.	2.6	134

#	Article	IF	CITATIONS
235	Concentration Dependent Scattering Coefficients of Intralipid Measured with OCT. , 2010, , .		1
236	Measurements of Wavelength Dependent Scattering Coefficients by Low Coherence Spectroscopy. , 2010, , .		0
237	Simultaneous imaging of ultrasound attenuation, speed of sound, and optical absorption in a photoacoustic setup. Proceedings of SPIE, 2009, , .	0.8	4
238	Real-time photoacoustic and ultrasound imaging of human vasculature. Proceedings of SPIE, 2009, , .	0.8	2
239	Millimeter-resolution acousto-optic quantitative imaging in a tissue model system. Journal of Biomedical Optics, 2009, 14, 034031.	2.6	6
240	A New Generation of Optical Diagnostics for Bladder Cancer: Technology, Diagnostic Accuracy, and Future Applications. European Urology, 2009, 56, 287-297.	1.9	127
241	Doppler calibration method for Spectral Domain OCT spectrometers. Journal of Biophotonics, 2009, 2, 407-415.	2.3	11
242	Imaging of tumor vasculature using Twente photoacoustic systems. Journal of Biophotonics, 2009, 2, 701-717.	2.3	73
243	Review of methodological developments in laser Doppler flowmetry. Lasers in Medical Science, 2009, 24, 269-283.	2.1	228
244	Review of laser speckle contrast techniques for visualizing tissue perfusion. Lasers in Medical Science, 2009, 24, 639-651.	2.1	296
245	Time domain algorithm for accelerated determination of the first order moment of photo current fluctuations in high speed laser Doppler perfusion imaging. Medical and Biological Engineering and Computing, 2009, 47, 1103-9.	2.8	6
246	Are quantitative attenuation measurements of blood by optical coherence tomography feasible?. Optics Letters, 2009, 34, 1435.	3.3	52
247	Quantitative measurements of absorption spectra in scattering media by low-coherence spectroscopy. Optics Letters, 2009, 34, 3746.	3.3	32
248	Twente Optical Perfusion Camera: system overview and performance for video rate laser Doppler perfusion imaging. Optics Express, 2009, 17, 3211.	3.4	55
249	Cell viability studies of PEG-thiol treated gold nanorods as optoacoustic contrast agents. , 2009, , .		11
250	Discrete dipole approximation simulations of gold nanorod optical properties: Choice of input parameters and comparison with experiment. Journal of Applied Physics, 2009, 105, .	2.5	84
251	Time domain algorithm for whole field laser Doppler perfusion imaging. , 2009, , .		0

252 Path length resolved optical Doppler flowmetry. , 2009, , .

0

#	Article	IF	CITATIONS
253	Diameter measurement from images of fluorescent cylinders embedded in tissue. Medical and Biological Engineering and Computing, 2008, 46, 589-596.	2.8	23
254	Photoacoustic imaging of portâ€wine stains. Lasers in Surgery and Medicine, 2008, 40, 178-182.	2.1	33
255	Speckle size and decorrelation time; space–time correlation analysis of coherent light dynamically scattered from turbid media. Optics Communications, 2008, 281, 1755-1760.	2.1	8
256	High angle phase modulated low coherence interferometry for path length resolved Doppler measurements of multiply scattered light. Optics Communications, 2008, 281, 494-498.	2.1	4
257	Wavelength swept Ti:sapphire laser. Optics Communications, 2008, 281, 4975-4978.	2.1	8
258	Imaging of acoustic attenuation and speed of sound maps using photoacoustic measurements. Proceedings of SPIE, 2008, , .	0.8	12
259	Combined Raman spectroscopy and optical coherence tomography device for tissue characterization. Optics Letters, 2008, 33, 1135.	3.3	104
260	Connecting laser Doppler perfusion imaging and laser speckle contrast analysis. , 2008, , .		4
261	Real-time in vivo photoacoustic and ultrasound imaging. Journal of Biomedical Optics, 2008, 13, 1.	2.6	133
262	Influence of tissue optical properties on laser Doppler perfusion imaging, accounting for photon penetration depth and the laser speckle phenomenon. Journal of Biomedical Optics, 2008, 13, 024001.	2.6	18
263	Photoacoustic imaging of tumor angiogenesis. Proceedings of SPIE, 2008, , .	0.8	2
264	Blood oxygen saturation of frozen tissue determined by hyper spectral imaging. Proceedings of SPIE, 2008, , .	0.8	1
265	Path-length-resolved optical Doppler perfusion monitoring. Journal of Biomedical Optics, 2007, 12, 060508.	2.6	9
266	Evaluation of a multimode fiber optic low coherence interferometer for path length resolved Doppler measurements of diffuse light. Review of Scientific Instruments, 2007, 78, 126103.	1.3	6
267	Speed-of-sound imaging in a photoacoustic imager. , 2007, , .		5
268	Path-length-resolved measurements of multiple scattered photons in static and dynamic turbid media using phase-modulated low-coherence interferometry. Journal of Biomedical Optics, 2007, 12, 024020.	2.6	27
269	Depth sensitivity of laser Doppler perfusion imager: quantification based on experiments and Monte Carlo simulations on static and dynamic scattering phantoms. , 2007, , .		0

270 $\,$ NAOMI: nanoparticle-assisted optical molecular imaging. , 2007, , .

#	Article	IF	CITATIONS
271	Photoacoustic imaging of port-wine stains. , 2007, , .		Ο
272	First clinical trials of the Twente photoacoustic mammoscope (PAM). , 2007, , .		2
273	Quantification of Doppler broadening in path length resolved diffusive light scattering using phase modulated low-coherence interferometry. , 2007, , .		0
274	Laser Doppler Perfusion Imaging with a high-speed CMOS-camera. Proceedings of SPIE, 2007, , .	0.8	4
275	Region-of-interest breast images with the Twente Photoacoustic Mammoscope (PAM). , 2007, , .		9
276	Acoustic property measurements in a photoacoustic imager. Proceedings of SPIE, 2007, , .	0.8	4
277	Reflection mode photoacoustic measurement of speed of sound. Optics Express, 2007, 15, 3291.	3.4	20
278	Quantification of optical Doppler broadening and optical path lengths of multiply scattered light by phase modulated low coherence interferometry. Optics Express, 2007, 15, 9157.	3.4	25
279	Effect of speckles on the depth sensitivity of laser Doppler perfusion imaging. Optics Express, 2007, 15, 10911.	3.4	2
280	Initial results of in vivo non-invasive cancer imaging in the human breast using near-infrared photoacoustics. Optics Express, 2007, 15, 12277.	3.4	260
281	Discrimination between Doppler-shifted and non-shifted light in coherence domain path length resolved measurements of multiply scattered light. Optics Express, 2007, 15, 13340.	3.4	11
282	Concomitant speed-of-sound tomography in photoacoustic imaging. Applied Physics Letters, 2007, 91, .	3.3	64
283	Synthesis and Bioconjugation of Gold Nanoparticles as Potential Molecular Probes for Light-Based Imaging Techniques. International Journal of Biomedical Imaging, 2007, 2007, 1-10.	3.9	105
284	Recent developments in optical coherence tomography for imaging the retina. Progress in Retinal and Eye Research, 2007, 26, 57-77.	15.5	304
285	Quantification of spatial intensity correlations and photodetector intensity fluctuations of coherent light reflected from turbid particle suspensions. Physical Review E, 2007, 75, 060901.	2.1	4
286	Speckles in laser Doppler perfusion imaging. Optics Letters, 2006, 31, 468.	3.3	31
287	Path length resolved Doppler measurements of multiple scattered photons in turbid media for various absorptions using phase modulated low-coherence interferometry. , 2006, , .		1
288	<title>Hematocrit-dependence of the scattering coefficient of blood determined by optical coherence</td><td></td><td>1</td></tr></tbody></table></title>		

tomography</title>., 2006, , .

4

#	Article	IF	CITATIONS
289	Temperature-dependent optical properties of individual vascular wall components measured by OCT. , 2006, 6078, 381.		0
290	Role of speckles in laser Doppler perfusion imaging: an investigation on particle suspensions. , 2006, , .		0
291	NAOMI: nanoparticle assisted optical molecular imaging. , 2006, , .		5
292	Mitochondrial PO2 measured by delayed fluorescence of endogenous protoporphyrin IX. Nature Methods, 2006, 3, 939-945.	19.0	148
293	In vivo photoacoustic imaging of blood vessels with a pulsed laser diode. Lasers in Medical Science, 2006, 21, 134-139.	2.1	138
294	Photoacoustic imaging of valves in superficial veins. Lasers in Surgery and Medicine, 2006, 38, 740-744.	2.1	13
295	Imaging of venous valves with photoacoustics. , 2006, , .		1
296	Temperature-dependent optical properties of individual vascular wall components measured by optical coherence tomography. Journal of Biomedical Optics, 2006, 11, 041120.	2.6	31
297	Characterization of a clinical prototype for photoacoustic mammography and some phantom studies. , 2005, , .		3
298	Discrimination of atherosclerotic plaque constituents based on local measurements of optical attenuation coefficents by OCT. , 2005, 5686, 426.		1
299	Discrimination of atherosclerotic plaque constituents based on local measurements of optical attenuation coefficients by OCT. , 2005, , .		0
300	Localized measurement of optical attenuation coefficients of atherosclerotic plaque constituents by quantitative optical coherence tomography. IEEE Transactions on Medical Imaging, 2005, 24, 1369-1376.	8.9	141
301	Optical coherence tomography of the Ex-PRESS miniature glaucoma implant. Lasers in Medical Science, 2005, 20, 41-44.	2.1	21
302	Quantitative optical coherence tomography of arterial wall components. Lasers in Medical Science, 2005, 20, 45-51.	2.1	52
303	The Twente Photoacoustic Mammoscope: system overview and performance. Physics in Medicine and Biology, 2005, 50, 2543-2557.	3.0	201
304	Serial noninvasive photoacoustic imaging of neovascularization in tumor angiogenesis. Optics Express, 2005, 13, 89.	3.4	219
305	Toward assessment of blood oxygen saturation by spectroscopic optical coherence tomography. Optics Letters, 2005, 30, 1015.	3.3	129

306 Curve fitting for quantitative measurement of attenuation coefficients from OCT images. , 2005, , .

#	Article	IF	CITATIONS
307	Apoptosis Induces Temporal Increase in Attenuation as Measured by Optical Coherence Tomography. , 2005, , .		0
308	Calculations of scattering by (de-)oxygenated whole blood. , 2004, , .		0
309	Oxygen Saturation-Dependent Absorption and Scattering of Blood. Physical Review Letters, 2004, 93, 028102.	7.8	222
310	Photoacoustic mammography laboratory prototype: imaging of breast tissue phantoms. Journal of Biomedical Optics, 2004, 9, 1172.	2.6	99
311	Photoacoustic imaging of blood vessels with a double-ring sensor featuring a narrow angular aperture. Journal of Biomedical Optics, 2004, 9, 1327.	2.6	52
312	Photoacoustic imaging of blood vessels in the chorioallantoic membrane of a chicken embryo. , 2004, ,		0
313	Photoacoustic determination of blood vessel diameter. Physics in Medicine and Biology, 2004, 49, 4745-4756.	3.0	79
314	Quantitative measurement of attenuation coefficients of weakly scattering media using optical coherence tomography. Optics Express, 2004, 12, 4353.	3.4	271
315	<title>Three-dimensional photoacoustic imaging of breast tissue phantoms</title> . , 2004, , .		2
316	Oxygen saturation dependent absorption and scattering of whole blood. , 2004, , .		3
317	Quantitative determination of localized tissue oxygen concentration in vivo by two-photon excitation phosphorescence lifetime measurements. Journal of Applied Physiology, 2004, 97, 1962-1969.	2.5	59
318	Low Coherence Spectroscopy (LCS) for depth resolved measurements of optical properties in tissue , 2004, , .		0
319	Measurement of the axial point spread function in scattering media using single-mode fiber-based optical coherence tomography. IEEE Journal of Selected Topics in Quantum Electronics, 2003, 9, 227-233.	2.9	129
320	Function and Structure of Pressurized and Perfused Porcine Carotid Arteries. American Journal of Pathology, 2003, 163, 1743-1750.	3.8	8
321	Light absorption of (oxy-)hemoglobin assessed by spectroscopic optical coherence tomography. Optics Letters, 2003, 28, 1436.	3.3	150
322	Photoacoustic monitoring and imaging of blood vessel size in vivo. , 2003, , .		2
323	Effects of absorption on coherence domain path length resolved dynamic light scattering in the diffuse regime. Applied Physics Letters, 2002, 81, 595-597.	3.3	18
324	UVB-activated Psoralen Reduces Luminal Narrowing After Balloon Dilation Because of Inhibition of Constrictive Remodeling¶. Photochemistry and Photobiology, 2002, 75, 68.	2.5	10

#	Article	IF	CITATIONS
325	Comparative optical coherence tomography imaging of human esophagus: How accurate is localization of the muscularis mucosae?. Gastrointestinal Endoscopy, 2002, 56, 852-857.	1.0	33
326	Notes on Past and Current Research at the Laser Centre in Amsterdam. Medical Laser Application: International Journal for Laser Treatment and Research, 2002, 17, 65-72.	0.3	0
327	UVB-activated Psoralen Reduces Luminal Narrowing After Balloon Dilation Because of Inhibition of Constrictive Remodeling¶. Photochemistry and Photobiology, 2002, 75, 68-75.	2.5	0
328	Comparative optical coherence tomography imaging of human esophagus: How accurate is localization of the muscularis mucosae?. Gastrointestinal Endoscopy, 2002, 56, 852-857.	1.0	34
329	High-flow-velocity and shear-rate imaging by use of color Doppler optical coherence tomography. Optics Letters, 1999, 24, 1584.	3.3	67
330	Adaptive STFT filtering to increase SNR in Color Doppler Optical Coherence Tomography. , 1999, , .		0
331	Saline flush during excimer laser angioplasty: Short and long term effects in the rabbit femoral artery. , 1998, 23, 128-140.		12
332	Psoralen and long wavelength ultraviolet radiation as an adjuvant therapy for prevention of intimal hyperplasia and constrictive remodeling after balloon dilation: A study in the rabbit iliac artery. , 1998, 23, 281-290.		4
333	Velocity-estimation accuracy and frame-rate limitations in color Doppler optical coherence tomography. Optics Letters, 1998, 23, 1057.	3.3	101
334	Torsion measurement of catheters using polarized light in a single glass fibre. Physics in Medicine and Biology, 1998, 43, 1049-1057.	3.0	6
335	Remodeling of the atherosclerotic arterial wall. Coronary Artery Disease, 1997, 8, 415-422.	0.7	8
336	Arterial remodeling after balloon angioplasty of the coronary artery: An intravascular ultrasound study. American Heart Journal, 1997, 134, 680-684.	2.7	7
337	Compensatory Enlargement in Coronary and Femoral Arteries Is Related to Neither the Extent of Plaque-Free Vessel Wall Nor Lesion Eccentricity. Arteriosclerosis, Thrombosis, and Vascular Biology, 1997, 17, 2617-2621.	2.4	16
338	Excimer laser induced bubble: Dimensions, theory, and implications for laser angioplasty. , 1996, 18, 381-390.		40
339	Partial vaporization model for pulsed midâ€infrared laser ablation of water. Journal of Applied Physics, 1995, 78, 564-571.	2.5	37
340	Pulsed Laser Ablation of Soft Tissue. , 1995, , 709-763.		23
341	Temperature dependence of the absorption coefficient of water for midinfrared laser radiation. Lasers in Surgery and Medicine, 1994, 14, 258-268.	2.1	196
342	Excimer laser ablation of soft tissue: a study of the content of rapidly expanding and collapsing bubbles. IEEE Journal of Quantum Electronics, 1994, 30, 1339-1345.	1.9	35

#	Article	IF	CITATIONS
343	Contribution of photothermal and photomechanical effects during tissue ablation by the XeCl-excimer laser. , 1994, , .		0
344	Intraluminal vapor bubble induced by excimer laser pulse causes microsecond arterial dilation and invagination leading to extensive wall damage in the rabbit Circulation, 1993, 87, 1258-1263.	1.6	152
345	Origin of arterial wall dissections induced by pulsed excimer and mid-infrared laser ablation in the pig. Journal of the American College of Cardiology, 1992, 19, 1610-1618.	2.8	137
346	Noncontact tissue ablation by Holmium: YSGG laser pulses in blood. Lasers in Surgery and Medicine, 1991, 11, 26-34.	2.1	129
347	Some Laser-Tissue Interactions in 308 nm Excimer Laser Coronary Angioplasty. Journal of Interventional Cardiology, 1990, 3, 231-241.	1.2	23
348	Modified Fiber Tips for Laser Angioplasty: Mechanisms of Action. Journal of Interventional Cardiology, 1990, 3, 243-253.	1.2	5